PRAMANA — journal of physics

Vol. 78, No. 4
April 2012
pp. 613–623

Three-dimensional simulation of laser–plasma-based electron acceleration

A UPADHYAY[1,*], K PATEL[2], B S RAO[1], P A NAIK[1] and P D GUPTA[1]

[1]Laser Plasma Division, Raja Ramanna Centre for Advanced Technology, Indore 452 013, India
[2]Laser & Plasma Technology Division, Bhabha Atomic Research Centre, Mumbai 400 085, India
*Corresponding author. E-mail: ajitup@rrcat.gov.in

MS received 14 February 2011; revised 19 October 2011; accepted 8 November 2011

Abstract. A sequential three-dimensional (3D) particle-in-cell simulation code PICPSI-3D with a user friendly graphical user interface (GUI) has been developed and used to study the interaction of plasma with ultrahigh intensity laser radiation. A case study of laser–plasma-based electron acceleration has been carried out to assess the performance of this code. Simulations have been performed for a Gaussian laser beam of peak intensity 5×10^{19} W/cm^2 propagating through an underdense plasma of uniform density 1×10^{19} cm^{-3}, and for a Gaussian laser beam of peak intensity 1.5×10^{19} W/cm^2 propagating through an underdense plasma of uniform density 3.5×10^{19} cm^{-3}. The electron energy spectrum has been evaluated at different time-steps during the propagation of the laser beam. When the plasma density is 1×10^{19} cm^{-3}, simulations show that the electron energy spectrum forms a monoenergetic peak at ∼14 MeV, with an energy spread of ±7 MeV. On the other hand, when the plasma density is 3.5×10^{19} cm^{-3}, simulations show that the electron energy spectrum forms a monoenergetic peak at ∼23 MeV, with an energy spread of ±7.5 MeV.

Keywords. Laser–plasma simulation; PIC code; electron acceleration.

PACS Nos 52.38.Kd; 52.65.Rr; 41.75.Jv

1. Introduction

Recent advances in laser technology have led to the development of compact multi-terawatt and petawatt pulsed laser systems [1–4] in several laboratories worldwide. The interaction of these ultrashort, ultrahigh intensity laser pulses with a plasma has revealed fascinating physical phenomena and led to advances in areas such as ultrashort X-ray generation [5], high harmonic generation [6], electron acceleration [7–11] and ion acceleration [12,13]. Out of these, electron acceleration has drawn considerable attention due to the possibility of developing a compact table-top accelerator. High-intensity laser pulses propagating through an underdense plasma produce accelerating fields up to ∼100 GV/m over several millimetres and up to ∼1 TV/m over a few microns, which have been used

to accelerate electrons to an energy up to 170 MeV [9–11]. Since the accelerating gradient is 1000 times greater than that produced by conventional accelerator technology, laser–plasma-based acceleration has the potential of setting up compact accelerators in the future, the only limitation being the acceleration length. Experiments in several laboratories worldwide using gas jets have demonstrated acceleration of monoenergetic electrons of energy exceeding 10 MeV and narrow divergence using diverse laser and plasma parameters [14–21]. To increase the interaction length, plasma channels [10] and larger laser spots [9,11] were used and electron bunches at $\sim$0.1 GeV were produced. By extending the interaction length to the centimetre scale using a plasma channel, 0.5 GeV stable acceleration has been observed [21]. Improvement in the stability and control of electron beam energy has been demonstrated through controlled electron injection in two counterpropagating laser pulses [22] or by using a steady-state-flow gas cell [23].

Knowledge of the detailed electron bunch kinetics will be essential as the channel length and electron energy scales up. Simulations have an edge over analytical theory in explaining nonlinear plasma response, electron trapping and self-consistent acceleration. They provide insight into the internal dynamics to optimize LWFAs and are essential in modelling the physics of monoenergetic electron bunches from self-trapped electrons, observed in experiments of recent years, and evaluating the scaling of these experiments to higher energies [10,13,23–25]. Several laboratories have set up particle-in-cell (PIC) codes for such studies, e.g. VLPL [26,27], OSIRIS [28], VORPAL [29], and the behaviour predicted by these codes has been subsequently verified in several experiments. A multipurpose 3D PIC code named PICPSI-3D has been developed at the Laser & Plasma Technology Division, Bhabha Atomic Research Centre, Mumbai, India, to study the interaction of plasmas with laser and particle beams. In this PIC code, an intense laser pulse interacts with preformed plasma, and the evolution of the plasma and the field parameters can be studied. The code has been upgraded to facilitate the study of laser–plasma-based electron acceleration. In this paper, we present a case study of laser–plasma-based electron acceleration, carried out to assess the performance and limitations of the code. Simulations have been performed for a Gaussian laser beam of 5×10^{19} W/cm^2 peak intensity propagating through an underdense plasma of 1×10^{19} cm^{-3} uniform density, and for a Gaussian laser beam of 1.5×10^{19} W/cm^2 peak intensity propagating through an underdense plasma of 3.5×10^{19} cm^{-3} uniform density.

The code clearly demonstrates monoenergetic electron acceleration in both the cases. In the first case, the monoenergetic electrons have an energy peak at 16 MeV and an energy spread of $\pm$7 MeV with the tail extending up to 50 MeV. In the second case, the electrons have a monoenergetic peak at 23 MeV with an energy spread of $\pm$7.5 MeV with the tail extending up to 87 MeV.

2. The code

The code 'particle-in-cell plasma simulation-3D' (PICPSI-3D) uses the standard relativistic particle push and a local finite-difference time-domain (FDTD) solution to the full Maxwell equations. The code permits different plasma shapes (rectangular, cylindrical and spherical) and density variations (Gaussian, linear and tangent hyperbolic). The laser pulse can have a rectangular or a Gaussian temporal profile. The code has diagnostics for

the evolution of the electromagnetic fields, particle densities, energies and momenta. This is a sequential code with a static simulation box, written in C and C++ under the Linux platform. It uses the fast-light-toolkit (FLTK) and OpenGL libraries for the graphical-user interface and visualization of the data. There are a post-processor 'Picvic' and a movie viewer 'Moview' as accompanying utilities. The post-processor analyses the data at a given time-step and the movie viewer displays the frames saved from the two windows, namely 'particle field window' and 'particle density window' as an animated GIF movie.

The code has been modified to facilitate the study of laser–plasma-based electron acceleration, and has been commissioned on a dual processor (Quad Core Xeon, 3 GHz) workstation with 32 GB system memory. The code is run for simulations of laser–plasma-based electron acceleration for the parameters discussed in §3. We observe monoenergetic electron acceleration in short as well as long laser pulses, where the long laser pulse gets strongly self-phase modulated resulting in monoenergetic electron acceleration. The results are discussed in §4, in terms of the simulation parameters.

3. Simulation parameters

For our simulation study, plasma densities were taken keeping in view the parameters of our recent experiments on laser wakefield acceleration (LWFA) [30]. A rectangular simulation box with a pre-formed plasma of uniform density inside was chosen. A linearly polarized Gaussian laser pulse enters the simulation box from the left-hand side and propagates along the z-axis. The threshold for self-focussing of a laser beam in a plasma is given by $P_{\rm crit} \geq 17\,(\omega_{\rm L}/\omega_{\rm P})^2$ GW [8,31], where $\omega_{\rm L}$ is the laser frequency and $\omega_{\rm P}$ is the plasma frequency. For both the densities used in the simulations, the power of our laser (10 TW Ti:sapphire) was more than the critical power. The dephasing length, over which the electrons outrun the accelerating wakefield, is given by $(n_{\rm c}/n_{\rm e})^{3/2}\,\lambda_{\rm L}$ [32], and the maximum energy of the accelerated electrons is given by $2(n_{\rm c}/n_{\rm e})m_0c^2$ [14]. The Rayleigh range of the focussing optics in our experiment was about 250 μm [33]. The code has been run for two sets of laser and plasma parameters.

In the first case, the laser pulse ($\lambda = 790$ nm, $\tau_{\rm L} = 45$ fs) is focussed on to a spot of 5 μm (FWHM) in a plasma of density 1×10^{19} cm^{-3} with six macroparticles per cell, which is reasonable for the number of particles in tri-linear interpolation of particle weighting. The plasma consisted of 2×10^7 macroparticles and was inside a simulation box of $30 \times 30 \times 100$ μm^3 volume, with a mesh size of 0.1 μm. Initially, a laser pulse of intensity $\sim 3 \times 10^{18}$ W/cm^2 ($a_0 = 2$) was taken. The code was run for 6000 time-steps, with each time-step being 0.0962 fs. For the given plasma density, the dephasing length was $\sim$1800 μm, the critical power for self-focussing was 2.9 TW and the expected maximum electron energy was 170 MeV. The evolution of the longitudinal electric field, electron density, electron energy and the momentum phase-space was recorded after every 100 time-steps. The run took $\sim$21 days to simulate as a stand-alone job on the workstation. This run yielded no acceleration over the interaction length of 100 μm of the simulation box. The laser intensity was then increased to 5×10^{19} W/cm^2 ($a_0 = 34$), and the code was run keeping the remaining parameters unchanged. In this case, $\lambda_{\rm p}$ ($\sim$10.4 μm) $< c\tau_{\rm L}$ ($\sim$13.5 μm). Hence the acceleration is supposed to be in self-modulated wakefield regime.

In the second case, a laser pulse of intensity $\sim 1.5 \times 10^{19}$ W/cm^2 ($a_0 = 10$), $\tau = 18$ fs was focussed onto a 10 μm spot in a plasma of 3.5×10^{19} cm^{-3} density. The plasma consisted of 7×10^7 macroparticles ($\sim$4 macroparticles per cell) and was inside a simulation box of $25 \times 25 \times 260$ μm^3 volume, with a mesh size of 0.1 μm. The code was run for 11,000 time-steps, with each time-step being 0.0962 fs. The dephasing length in this case was $\sim$255 μm, the critical power for self-focussing was 0.8 TW and the expected maximum electron energy was 46 MeV. The evolution of the longitudinal electric field, electron density, electron energy and momentum phase-space was recorded after every 100 time-steps. The run took $\sim$72 days to simulate as a stand-alone job on the workstation. This case is clearly in the bubble regime as λ_p ($\sim$5.4 μm) $= c\tau_L$. A brief description of the results for both the cases is given in the next section.

4. Results

4.1 *Case* 1

In figure 1, one observes the growth of a clear bubble after 3400 time-steps ($\sim$327 fs). The figure shows a 2D slice of electron charge density along the $\hat{y}$–$\hat{z}$ central plane of the simulation box, where $\hat{y}$ is the direction of laser polarization and $\hat{z}$ is the direction of propagation of laser pulse. The electrons are shown in blue colour, and one observes gradual formation of a cavity-like structure devoid of electrons. In 3D, the structure takes the shape of a bubble. In this case, the long Gaussian laser pulse starts getting self-modulated

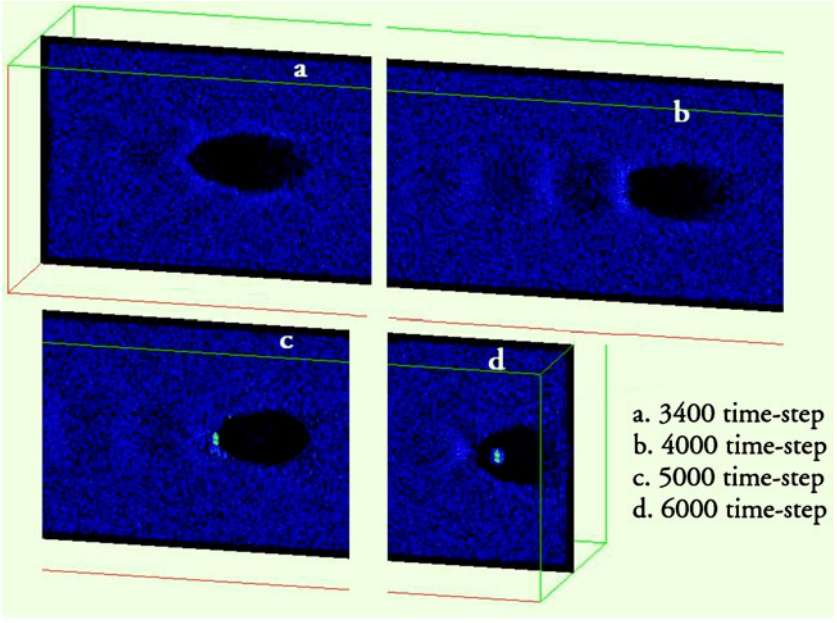

Figure 1. The electron density plot along the central plane of the simulation box for Case 1.

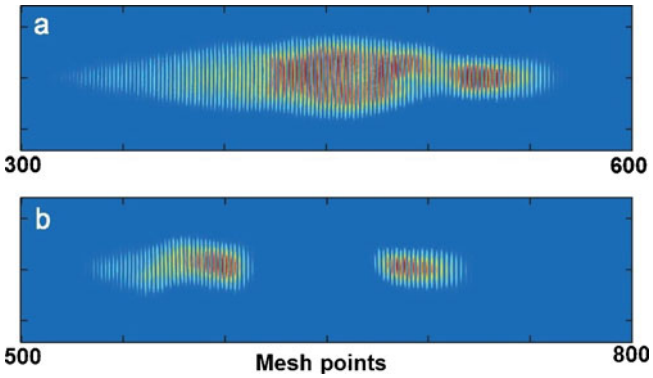

Figure 2. The self-modulated laser pulse inside the simulation box at (**a**) 3000 and (**b**) 5000 time-steps.

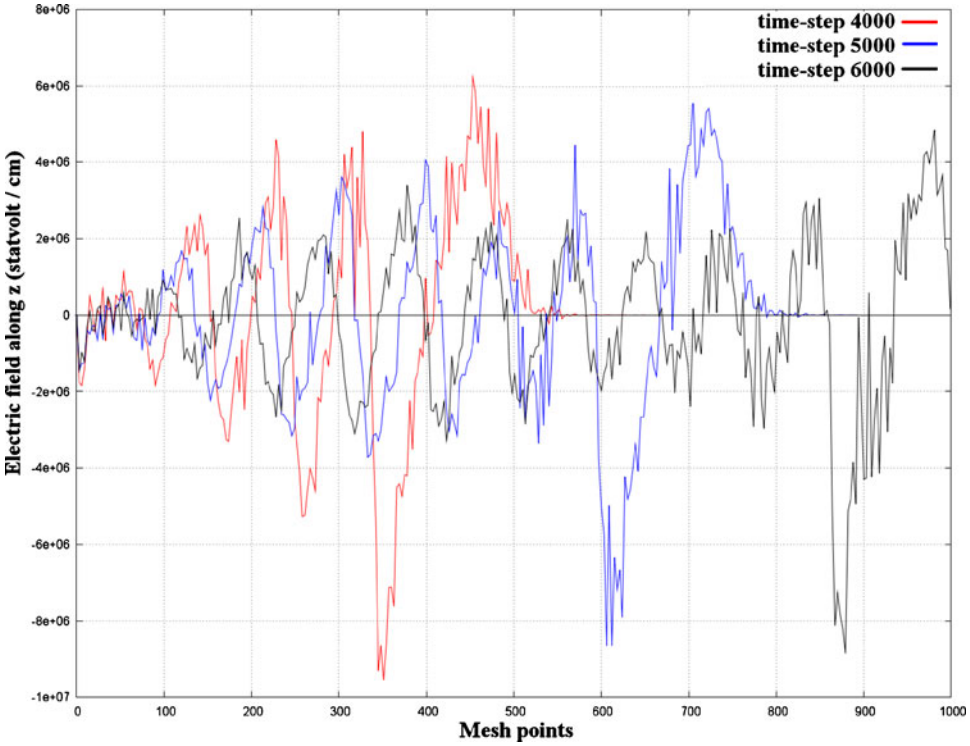

Figure 3. Longitudinal electric field (E_z) as a function of propagation distance z for Case 1.

at plasma period (∼105 mesh points) as shown in figure 2. The pulse is modulated in only two fragments as its length is marginally longer compared to the plasma wavelength. In the experiment, the occurrence of self-modulation was confirmed from the observation of the Stokes satellite in the FRS spectrum (figure 2a of [33]).

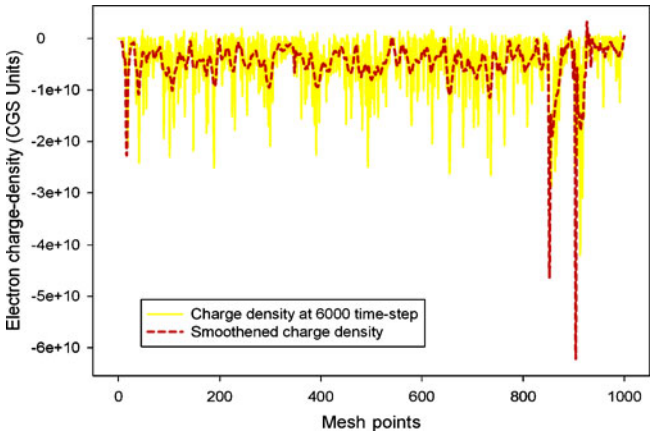

Figure 4. The electron charge density along z direction, at the central plane of the simulation box for Case 1.

Figure 3 shows the longitudinal electric field (E_z) as a function of propagation distance z. One can see the development of a bubble-like structure at 4000 time-steps between 300 and 500 mesh points along the z-axis. A sudden increase in the field amplitude at these time-steps is a signature of the bubble. As seen in the figure, the field indicates a bubble-like structure at 4000 time-steps between 350 and 450 mesh points, which has advanced between mesh points 600–700 at 5000 time-steps. One also observes that the field amplitude decreases slightly as the electrons are launched at 5000 time-steps. From figure 3 one infers that the field is $\sim$140 GV/cm, and the electrons are accelerated inside the bubble. Figure 4 shows the modulation of electron charge density at 6000 time-steps (577 fs) along the z-axis. From the figure, one observes that the electron charge density around 850 mesh points has increased to $\sim 5 \times 10^{10}$ from the background charge density of less than 1×10^{10}, whereas at a mesh point of $\sim$900, it has increased to 6×10^{10}, with a decrease in the charge density to almost zero in between. This again confirms the formation of a bubble with five and six times increase in the density at the rear and front of the bubble and a void in between.

The momentum phase-space plot is shown in figure 5. It is observed that initially the electrons acquire a momentum in the transverse field direction. With the build-up of the

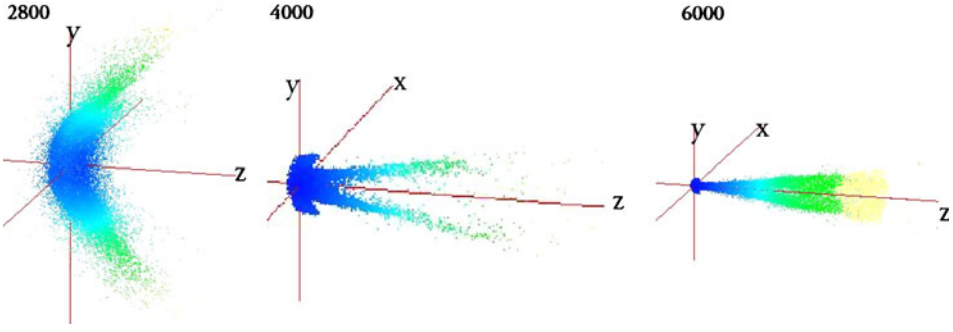

Figure 5. The momentum phase-space plot of electrons for Case 1.

longitudinal field, they start gaining longitudinal momentum resulting in the total momentum of electrons tilting along z-direction, and by the time the laser pulse has traversed 6000 time-steps, the electrons form a monoenergetic peak. Figure 6 shows the electron energy spectrum for three time-steps 5000, 5400 and 6000. It is evident that as the electrons are launched into bubble at time-step 5000 (481 fs), the electron energy spectrum starts forming a peak. It forms a clear peak at 16 MeV at 6000 time-steps (577 fs), with an energy spread of ± 7 MeV, where the tail of the spectrum extends up to 50 MeV. Our simulation box ends at 100 μm at 6000 time-steps. Due to limitations in system memory, we could not use a longer interaction length. Nevertheless, it is clear that a greater interaction length would have resulted in further gain in electron energy along with a sharpening of the electron energy peak. The full cone angle divergence of all the accelerated electrons comes out to be 0.23 radians, whereas the full cone angle for monoenergetic electrons is 0.0173 radians.

4.2 *Case* 2

In figure 7, one observes the growth of a clear bubble after 1600 time-steps ($\sim$154 fs). The bubble breaks at 4000 time-steps (384 fs) resulting in the launch of electrons inside the bubble. At 6800 time-steps (654 fs), the electron energy spectrum starts to show a peak.

Figure 8 shows longitudinal electric field amplitudes for three time-steps of 6400, 6800 and 7600. A sudden increase in the field amplitude at these time-steps is a signature of the bubble, and one infers that the field is $\sim$760 GV/cm. At 7600 time-steps, the bubble gets deformed. Figure 9 shows the modulation in electron charge density and one observes that the electron charge density around the mesh points 1420 and 1450 has increased to $\sim 5 \times 10^{11}$ from the background charge density of less than 0.2×10^{11}, with a decrease

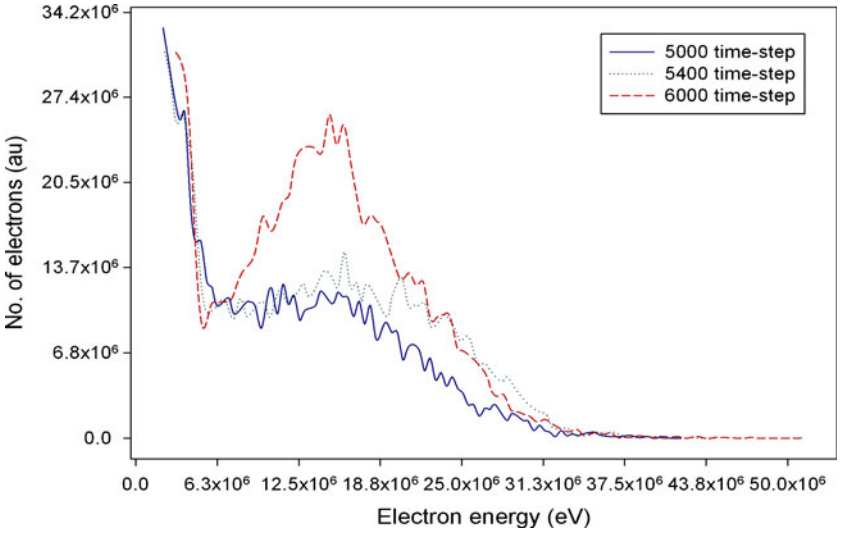

Figure 6. Electron energy spectrum for Case 1.

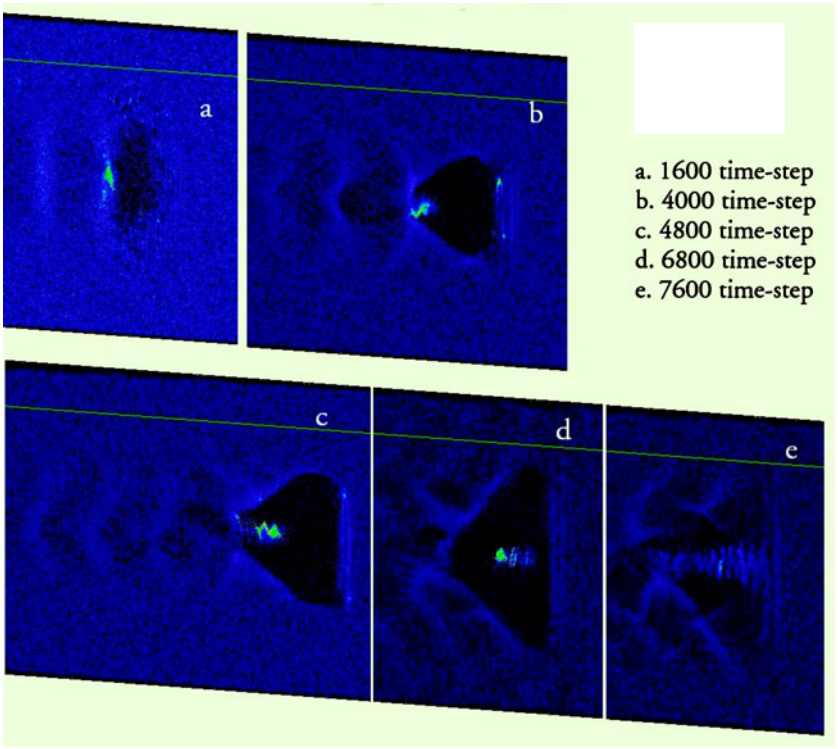

Figure 7. The electron density plot at the central plane of the simulation box for Case 2.

in the charge density to very low value in between. This again confirms the formation of a bubble with a strong increase in the density at the rear and front of the bubble and a void in between. Figure 10 shows the electron energy spectrum. It is evident that as the electrons are launched into the bubble at 4000 time-steps, the electron energy spectrum starts forming a peak at this time-step. It forms a clear peak at 23 MeV energy at 6400 time-steps, with an energy spread of ± 7.5 MeV, whereas the tail of the spectrum extends up to 87 MeV. The full cone angle divergence of all the accelerated electrons comes out to be 0.37 radians, whereas the full cone angle for monoenergetic electrons is 0.0736 radians.

Direct comparison of electron energy spectra with our experimental result is not possible as we could simulate only a part of the interaction length due to the serial nature of the code and limitation of system memory. However, the results of our simulation Case 1, qualitatively agrees with our experimental results, where one observes a monoenergetic peak even with a long pulse. This is due to the self-modulation of laser pulse where strong self-modulation of laser pulse leads to bubble-like structure.

Even though our simulation parameters are restricted by the limitations in the computing hardware, our results are in line with the reported results. The electron energy spectrum showing a continuum at initial time-step, and subsequently forming a peak

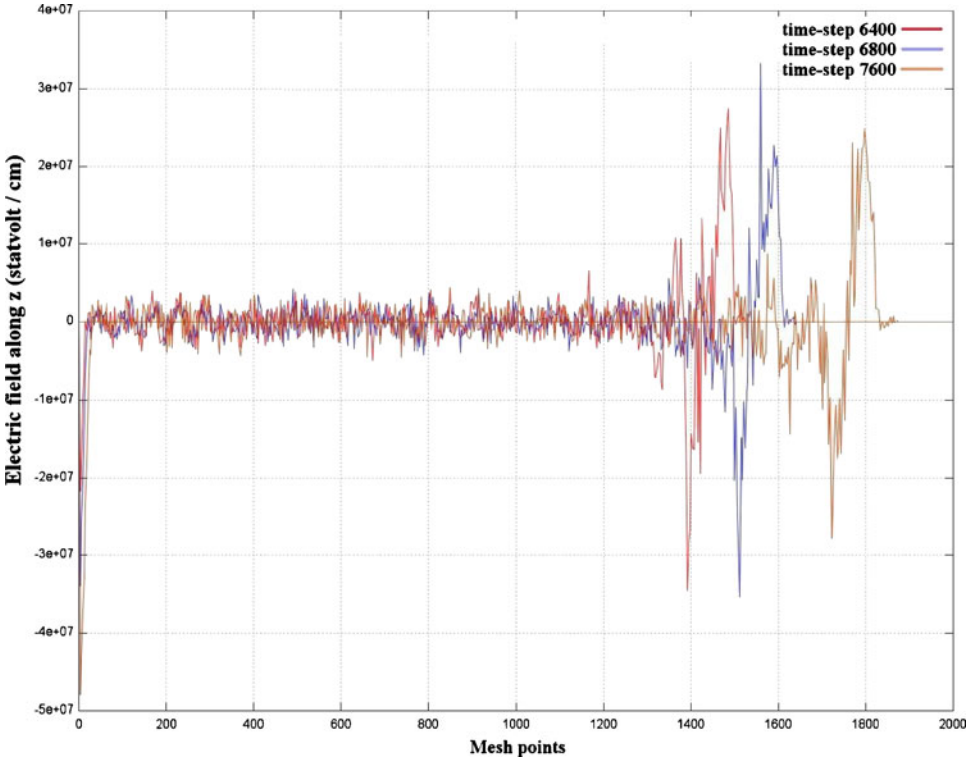

Figure 8. Longitudinal electric field (E_z) as a function of propagation distance z for Case 2.

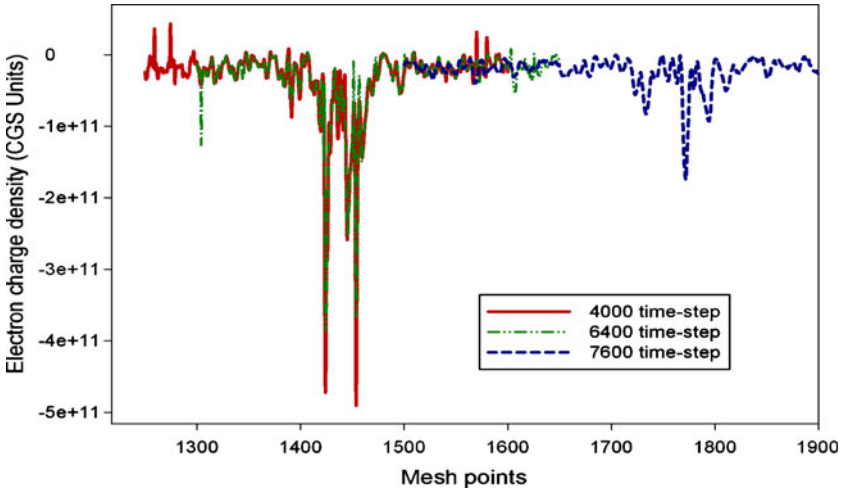

Figure 9. The electron charge density along z direction, at the central plane of the simulation box for Case 2.

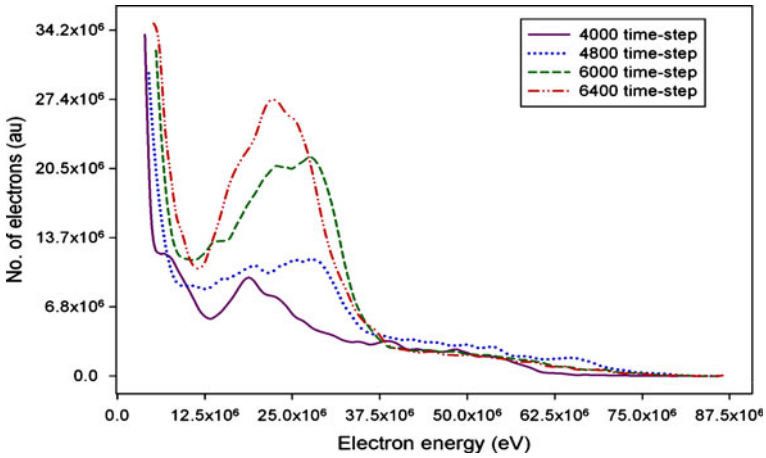

Figure 10. Electron energy spectrum at different time-steps for Case 2.

which narrows down and grows in amplitude at later time-steps has been reported by Pukhov *et al* using the code VLPL [14,34–36]. The typical simulation of a laser–plasma experiment with the VLPL code in the 3D geometry takes 24 h on 256 processing elements with 32 GB of memory [15]. The code PICPSI-3D has similar features as that of VLPL as it supports the interaction of a laser or particle beam with pre-formed plasma. However, the major difference is that our code is a serial code with static window, whereas VLPL is a fully parallel code with moving window. This differentiates the computational capabilities of two codes. On a single-processor workstation (devoted and with 32 GB memory) a similar simulation for a single parameter set would take about 1 year of CPU time.

In view of this, we plan to use a parallel version of PICPSI-3D on a cluster of four high-end devoted workstations with 104 GB memory each and 28 processing elements in total. This will enable us to go for higher plasma volume, lower number of electrons per macroparticle, smaller mesh size and probably better simulation results.

5. Conclusion

In conclusion, a sequential, 3D, PIC code for studying laser–plasma-based electron acceleration has been set up in our simulation laboratory. Laser–plasma-based electron acceleration has been studied on this code. We have simulated two regimes, namely, the SMLWFA regime and the bubble regime of acceleration. In the first regime, the laser pulse length is longer than the plasma wavelength, whereas, in the second regime, the laser pulse length equals the plasma wavelength. We observe that even in the SMLWFA regime, the choice of a very high intensity laser pulse results in bubble formation and leads to monoenergetic acceleration, which is common for the second regime. It is observed that the electrons are accelerated up to an energy of $\sim$ 50 MeV with a monoenergetic peak at 14 MeV for the first case. In the second case, electrons are accelerated up to an energy of $\sim$87 MeV with a monoenergetic peak at 23 MeV. The formation of a bubble is

confirmed from charge density snaps along the central plane of the simulation box. The same is also verified by the electron density plot at the central line of the simulation box and the plot of longitudinal electric field.

References

[1] M D Perry and G Mourou, *Science* **264**, 5161 (1994)
[2] V Yanovsky *et al*, *Opt. Exp.* **16**, 3 (2008)
[3] M D Perry *et al*, *Opt. Lett.* **24(3)**, 160 (1999)
[4] M Aoyama *et al*, *Opt. Lett.* **28(17)**, 1594 (2003)
[5] Y Jiang *et al*, *J. Opt. Soc. Am.* **B20**, 1 (2003)
[6] B Dromey *et al*, *Nature Phys.* **2**, 456 (2006)
[7] T Tajima and J M Dawson, *Phys. Rev. Lett.* **43**, 267 (1979)
[8] A Modena *et al*, *Nature* **377**, 606 (1995)
[9] S P D Mangles *et al*, *Nature* **431**, 535 (2004)
[10] C G R Geddes, C S Toth, J Van Tilborg, E Esarey, C B Schroeder, D Bruhwiler, C Nieter, J Cary and W P Leemans, *Nature* **431**, 538 (2004)
[11] J Faure, Y Glinec, A Pukhov, S Kiselev, S Gordienko, E Lefebvre, J-P Rousseau, F Burgy and V Malka, *Nature* **431**, 541 (2004)
[12] M Borghesi *et al*, *Fusion Sci. Technol.* **49**, 412 (2006)
[13] V Malka *et al*, *Nature Phys.* **4**, 447 (2008)
[14] A Pukhov and S Gordienko, *Phil. Trans. R. Soc.* **A364**, 623 (2006)
[15] A Pukhov, *MPQ-Report on High Performance 3D PIC Code VLPL: Virtual Laser Plasma Lab*
[16] E Miura, K Koyama, S Kato, N Saito, M Adachi, Y Kawada, T Nakamura and M Tanimoto, *Appl. Phys. Lett.* **86**, 251501 (2005)
[17] A Yamazaki *et al*, *Phys. Plasmas* **12**, 093101 (2005)
[18] T Hosokai *et al*, *Phys. Rev.* **E73**, 036407 (2006)
[19] C-H Hsieh, C-M Huang, C-L Chang, Y-C Ho, Y-S Chen, J-Y Lin, J Wang and S-Y Chen, *Phys. Rev. Lett.* **96**, 095001 (2006)
[20] B Hidding *et al*, *Phys. Rev. Lett.* **96**, 105004 (2006)
[21] M Mori *et al*, *Phys. Lett.* **A356**, 146 (2006)
[22] W P Leemans *et al*, *Nature Phys.* **2**, 696 (2006)
[23] J Osterhoff, *Phys. Rev. Lett.* **101**, 085002 (2008)
[24] W P Leemans *et al*, *Nature Phys.* **2**, 696 (2006)
[25] P A Naik and P D Gupta, *Int. J. Mod. Phys.* **B21**, 459 (2007)
[26] C Nieter, *J. Comp. Phys.* **196**, 448 (2004)
[27] C K Birdsall and A B Langdon, *Plasma physics via computer simulation* (McGraw-Hill, New York, 1985)
[28] R A Fonseca *et al*, *Lecture notes in computer science* (Springer, Berlin, 2002) Vol. 2331
[29] K S Yee, *IEEE Trans. Ant. Prop.* **14**, 302 (1966)
[30] J P Boris, *Proc. 4th Conf. Num. Sim. Plasmas* edited by J P Boris and R A Shanny (Naval Research Lab, Washington, DC, 1970) pp. 3–67
[31] R Bingham *et al*, *Plasma Phys. Control. Fusion* **46**, R1 (2004)
[32] J Villasenor and O Buneman, *Comput. Phys. Commun.* **69**, 306 (1992)
[33] S R Bobbili, A Moorti, P A Naik and P D Gupta, *New J. Phys.* **12**, 045011 (2010)
[34] A Pukhov and J Meyer-ter-Vehn, *Phys. Rev. Lett.* **76**, 3975 (1996)
[35] A Pukhov and J Meyer-ter-Vehn, *Phys. Rev. Lett.* **79**, 2686 (1997)
[36] A Pukhov and J Meyer-ter-vehn, *Appl. Phys.* **B74**, 355 (2002)